ANALYSIS OF THE NOVEMBER 1999 DEAD SEA CALIBRATION SHOTS

Arthur Rodgers, Stephen Myers, Kevin Mayeda and William Walter
Lawrence Livermore National Laboratory, Livermore, CA 94551 USA

Sponsored by U.S. Department of Energy
Office of Nonproliferation Research and Engineering
Office of Defense Nuclear Nonproliferation
National Nuclear Security Administration

Contract No. W-7405-ENG-48

ABSTRACT

In November 1999 three chemical explosions were conducted in the Dead Sea for the purposes of calibrating the International Monitoring System (IMS) for the Comprehensive Nuclear-Test-Ban Treaty (CTBT). These shots were organized and conducted by the Geophysical Institute of Israel (GII). Large chemical explosions are the most valuable form of ground truth as the location, depth and origin time are very well known. We focus on the two largest shots ($M_W \geq 3.6$) and performed several types of analysis of the regional recordings and travel times of these shots. These data provide valuable new information about the region and offer an opportunity to test monitoring strategies.

1) A crustal and uppermost mantle velocity model was inferred from the travel times of the regional phases: Pn, Pg and Sg. This effort utilized a grid search method to find suitable models of the structure. Results indicate that the crust is relatively thin (32 km) with lower than average crustal velocities (mean V_P = 6.1-6.2 km/s).

2) We located each shot treating the other shot as a calibration explosion. Locations were computed using both station static corrections and kriged correction surfaces. Results show that the locations with static corrections can be better or worse than the locations without corrections. However, the locations with kriged correction surfaces are consistently better than those without corrections or with static corrections because kriging properly accounts for residual statistics.

3) Measures of the S-wave coda for regional events provide a stable estimate of event size (moment magnitude, M_W) and the event source spectrum. S-wave coda envelope amplitudes were calibrated to moments estimated from long-period waveform modeling. We measured moment and body-wave magnitudes and source spectra for many events in the region. The Dead Sea shots show spectral peaking associated with shallow events.

4) Finally, analysis of regional broadband recordings from the Saudi Arabian National Seismic Network reveals spectral scalloping associated with the bubble pulse. The observed bubble pulse periods are consistent with theoretical predictions.

Research performed under the auspices of the U.S. Department of Energy by the Lawrence Livermore National Laboratory under contract W-7405-ENG-48. LLNL contribution UCRL-JC-138997.

Key Words: 1999 Dead Sea Shots, calibration shots, regional velocity models, regional location, regional discrimination

OBJECTIVE

The use of calibration explosions for seismic monitoring of a Comprehensive Nuclear-Test-Ban Treaty (CTBT) provides valuable empirical data and opportunities to test monitoring strategies. Calibration explosions offer a unique set of travel time and explosion source data of the highest quality of ground truth because the source location, depth and origin time are precisely known. For this reason calibration explosions are widely viewed to be the most desirable type of source for empirical calibration.

We analyzed seismic data from the November 1999 Dead Sea Shots to investigate several aspects of regional seismic monitoring. Travel times were used to develop a one-dimensional regional model for event location. Travel time correction methodologies and their effect on event location were tested. Regional S-wave coda moment magnitudes, M_W, scale were computed. Analysis of the source spectrum from S-wave coda waves revealed spectral peaking. This study makes use of the unique data set that the Dead Sea shots provided and demonstrates the importance and potential value of future calibration explosions.

RESEARCH ACCOMPLISHED

This study reports analysis of regional travel-time and waveform data from the November 1999 Dead Sea Shots to address several different aspects of regional seismic monitoring. Each aspect will be presented in its own section. A brief description of the shots follows.

Dead Sea Shots and Regional Seismic Data

In November of 1999, the Geophysical Institute of Israel (GII) conducted three chemical explosions in the Dead Sea. These explosions were conducted to provide calibration data for seismic travel times to stations of the International Monitoring System (IMS) to improve detection and location efforts for CTBT monitoring. Details of the shot locations and origin times are compiled in Table 1. The two largest shots (m_b 3.45 and 3.6) were well observed out to regional distances ($\Delta \geq 500$ km). The Middle East has dense coverage of seismic stations due to the relatively high population density and earthquake hazard along the Gulf of Aqaba-Dead Sea Rift. Stations operated by regional networks in Israel (GII), Jordan (Jordanian Seismic Observatory, JSO), Syria and Saudi Arabia (King Abdulaziz City for Science and Technology, KACST and King Saud University, KSU) were operating during the shots. A map of the shot and station locations is shown in Figure 1.

One-Dimensional Velocity Model Development

The travel times of first-arriving P-waves (Pn and Pg) were used to develop an average one-dimensional velocity model of the crust and uppermost mantle for the region. The P-waves were picked from waveforms from the Jordanian and Saudi Arabian networks. Waveforms were not available for all stations and some waveforms were discarded due to poor signal-to-noise levels. Sn was not clearly observed for these data, including the horizontal components of the KACST network stations. Sn is not expected to propagate efficiently along the paths studied (Kadinsky-Cade et al., 1981; Rodgers et al., 1997). Sg propagated efficiently and was picked when clearly observed.

Firstly, we regressed the travel times of each phase versus distance. Data from both shots were included in this analysis. Both explosions have very similar travel times to each station suggesting that there are not timing errors at the stations between the two shots, although picking the phases can be difficult because of poor signal-to-noise levels. Figure 2a shows the Pn, Pg and Sg travel times versus distance and regression fits for the recordings in Saudi Arabia. The slopes of the Pg and Sg travel times versus distance should reflect the average P- and S-wave velocities of the crust, while the Pn travel-time slope should indicate the average sub-Moho P-wave velocity, assuming the Moho is flat. However, caution must be exercised because two-dimensional structure along the path could bias the results. In fact analysis of seismic refraction data sampling the Sinai Peninsula margin of the Gulf of Aqaba indicates that crust thins from about 30 km north of the Gulf of Aqaba to 20 km at the southern-most tip of the Peninsula (Ginzburg et al., 1979). A low average Pn velocity (7.8 km/s) is reported for the Dead Sea Rift by the seismic refraction

study of Ginzburg et al., (1979) and the Pn tomography study of Hearn and Ni (1994). The absence of short-period Sn propagation in the region and low Pn velocities is consistent with the presence of partial melt in the shallow mantle. A crustal thickness of about 30 km for the Dead Sea region is reported from studies of seismic refraction data (Ginzburg et al., 1979) and teleseismic receiver functions (Sandvol, et al., 1998). Our goal is simply to estimate an adequate one-dimensional velocity model for the region.

We estimated a velocity model from the picked P-wave data shown in Figure 2b using a grid search scheme. A wide range of models was generated and the mean and root-mean square (rms) of the residuals (data minus model prediction) were computed. Models were chosen to minimize the absolute mean residual while also providing good scatter reduction. The sensitivity of travel times to one-dimensional (1D) average velocity structure is certainly non-unique and our goal is to find a range of models that fit the data reasonably well and are consistent with what is already known about the region. By using a grid search technique we avoid problems associated with linearizing the dependence of the data on model parameters, as is required by linear inversion methods. Because the calculation of travel times in a 1D model is fast, the grid search allows us to quickly investigate a wide range of models.

Figure 2c shows the models used in the grid search. We assumed a 2-km-thick sediment layer for all models. The total crustal thickness was varied from 24 to 34 km with a 2-km increment. Three layers composed the crystalline crust: an upper crust (5-km thickness, v_P = 5.0-5.4km/s, 0.1 km/s increment); a middle crust (5 km thickness, v_P = 5.7-6.2km/s, 0.1 km/s increment); and a lower crust (variable thickness, v_P = 6.2-7.0km/s, 0.2 km/s increment). The mantle P-wave velocity was set to 7.8 km/s, consistent with the regression value (Figure 2a).

The best-fitting 1% of the 900 models considered are shown in Figure 2c. The crustal thickness is 32 km for all these models. Upper crustal velocities are poorly constrained. The average crustal P-wave velocity for the best-fitting models is 6.1-6.2 km/s. The model is compiled in Table 2.

Event Relocation: Testing Travel-Time Corrections Methodologies

The two largest Dead Sea shots provide a unique opportunity to test travel time correction methodologies for event location. Each shot was treated as a calibration shot and travel time corrections were computed and applied while locating the other event. In each case we used the reported analyst picks (first-arriving P-waves) from all available regional stations (Figure 1). Two methodologies were used to compute travel-time corrections: station static delays (relative to a one-dimensional model) and kriged correction surfaces (Schultz et al., 1998). Figures 3a and 3b show the ground truth locations, the computed locations without corrections, and with both correction strategies. Results indicate that using the static corrections degraded the location of the Nov. 10 shot compared to the location without corrections. However, the location of the Nov. 11 shot with static corrections is closer to ground truth compared to the location without corrections. The locations with corrections from the kriged surface were closest to ground truth for both events.

The inconsistent behavior of locations using static delay times is due to picking errors. This is illustrated in Figure 3c where we show the individual residuals and kriged travel-time correction surface for both events. In a few cases individual stations have very different residuals, presumably due to inconsistent picking of the arrivals. Despite differences between residuals at a few stations for the two shots, the correction surfaces are generally in good agreement. Fluctuations between nearby data points that arise from picking errors can bias static delay time corrections. Kriging accounts for fluctuations in nearby data points by averaging through the points, leading to a smooth correction surface and more stable corrections.

S-wave Coda Magnitudes

Measurements from the S-wave coda have been shown to provide estimates of the seismic source spectrum and remarkably stable moment magnitudes (Mayeda and Walter, 1996). We measured envelopes of the S-wave coda at the broadband station MRNI in Israel (Figure 4). The estimated source spectra (Figure 4c) are peaked relative to that of a nearby earthquake. Spectral peaking arises from interference notches, Rg-to-S scattering and/or near-source attenuation effects. Yields of the smaller shots are estimated relative to the 5000-kg shot in the low frequency band (0.5-1.5 Hz) band to be 2036-kg and 570-kg for the Nov. 10 and

Nov. 8 shots. Single-station coda body-wave magnitudes, mb, are estimated from the 1-2 Hz band: 3.6, 3.45 and 2.95. Figure 4d shows the source spectra of the three shots scaled by yield. The spectra are similar for frequencies less than 1 Hz, but different for frequencies above 1 Hz. The spectra above 1 Hz do not agree because of source dimensions and bubble pulse interference.

Bubble Pulse Observations

Underwater explosions generate a primary (direct) pulse and secondary pulses associated with the expansion and contraction of a rising gas sphere, called the bubble pulse. Each bubble pulse acts like a secondary source and radiates acoustic energy into the water and this energy subsequently propagates into the solid crust. Due to interference of the direct and bubble pulse excitation, the far-field seismic response should reveal modulation (scalloping) in the spectrum. We observed a very consistent pattern of spectral modulation using the broadband stations of the Saudi National Seismic Network. Figure 5 shows the vertical component spectra and auto-correlations for six stations. Theoretical predictions of the bubble pulse frequency/period reported by GII are 1.72 Hz/0.583 s and 1.26 Hz/0.791 s for the November 10 and 11 shots, respectively. The observed bubble pulse frequencies are in good agreement with their predictions.

CONCLUSIONS AND RECOMMENDATIONS

The Dead Sea Shots provided valuable data for empirical travel-time calibration as well as testing regional seismic monitoring strategies. Unfortunately, the shots were not well recorded by single stations of the International Monitoring System (IMS) at teleseismic distances. Nonetheless, the shots can be used as calibration points for regional velocity models and travel time correction surfaces. We used the travel-times of first-arriving P-waves to estimate a one-dimensional average velocity model for the region. Using the two shots to test travel-time correction strategies for event location, we showed that kriging corrections provide locations closer to ground truth than station-based static delay times. Source spectra inferred from S-wave coda amplitudes show that the shot spectra are peaked below about 2 Hz. Broadband recordings of the shots show spectral scalloping associated with the bubble pulse.

Analysis of regional data from the Dead Sea Shots shows that such calibration shots can be used to successfully calibrate regional seismic travel times and test monitoring strategies. Future experiments can be conducted to advance empirical calibration of new regions.

ACKNOWLEDGEMENTS

AR is grateful to the staffs of KACST and KSU for their hospitality during a visit in November 1999 and for generously sharing waveform data.

REFERENCES

Ginzburg, A., J.Makris, K. Fuchs, C. Prodehl, W. Kaminski and U. Amitai (1979). A seismic study of the crust and upper mantle of the Jordan-Dead Sea Rift and their transition toward the Mediterranean Sea, *J. Geophys. Res*., 84, 1569-1582.

Hearn, T. and J. Ni (1994). Pn velocities beneath continental collision zones: the Turkish-Iranian Plateau, *Geophys. J. Int*., **117**, 273-283.

Kadinsky-Cade, K., M. Barazangi, J. Oliver and B. Issacks (1981). Lateral variations of high-frequency seismic wave propagation at regional distances across the Turkish and Iranian Plateaus, *J. Geophys. Res*., 86, 9377-9396.

Mayeda, K. and W. Walter (1996). Moment, energy, stress drop and source spectra of western United States earthquakes from regional coda envelopes, *J.Geophys.Res.*, **101**, 11,195-11,208.

Rodgers, A., J. Ni and T. Hearn (1997). Propagation characteristics of short-period Sn and Lg in the Middle East, *Bull. Seism. Soc. Am*., 87, 396-413.

Sandvol, E., D. Seber, A. Calvert and M. Barazangi (1998). Grid search modeling of receiver functions: Implications for crustal structure in the Middle East and North Africa, *J. Geophys. Res*., 103, 26,899.

Schultz, C, S. Myers, J. Hipp and C. Young (1998). Nonstationary Bayesian kriging: application of spatial corrections to improve seismic detection, location and identification, *Bull. Seism. Soc. Am.*, **88**, 1275-1288.

Table 1. Ground Truth Locations from Geophysical Institute of Israel

LATITUDE	LONGITUDE	DATE	TIME (GMT)	YIELD (KG TNT)
31.5330	35.4406	Nov. 8, 1999	13:00:00.33	500
31.5338	35.4400	Nov. 10, 1999	13:59:52.210	2060
31.5336	35.4413	Nov. 11, 1999	15:00:00.795	5000

These data were taken from the Geophysical Institute of Israel: http://www.gii.co.il.

Table 2. Preferred Velocity Model for the Region

DEPTH (KM)	THICKNESS(KM)	V_P (KM/S)	V_S (KM/S)
0.0	2	4.50	2.60
2	5	5.00	2.89
7	10	6.10	3.42
17	15	6.80	3.82
32	∞	7.80	4.38

V_P and V_S are the P- and S-wave velocities, respectively.

November 1999 Dead Sea Shots and Regional Seismic Stations

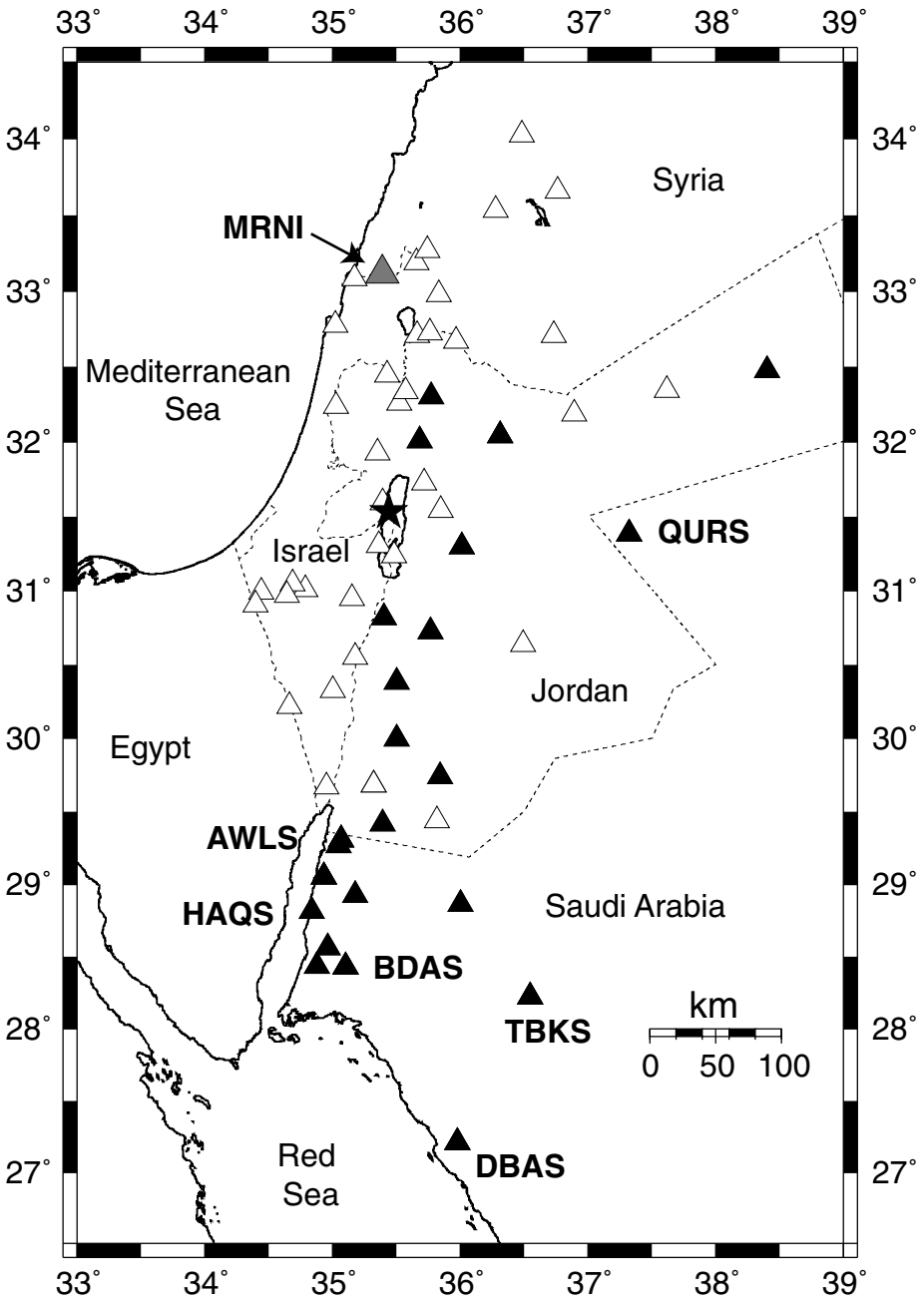

Figure 1. Map of the Dead Sea Shot locations (star) and regional seismic stations reporting P-wave picks (triangles). Black triangles indicate stations for which we had waveform data and picked phase arrivals for velocity model development.

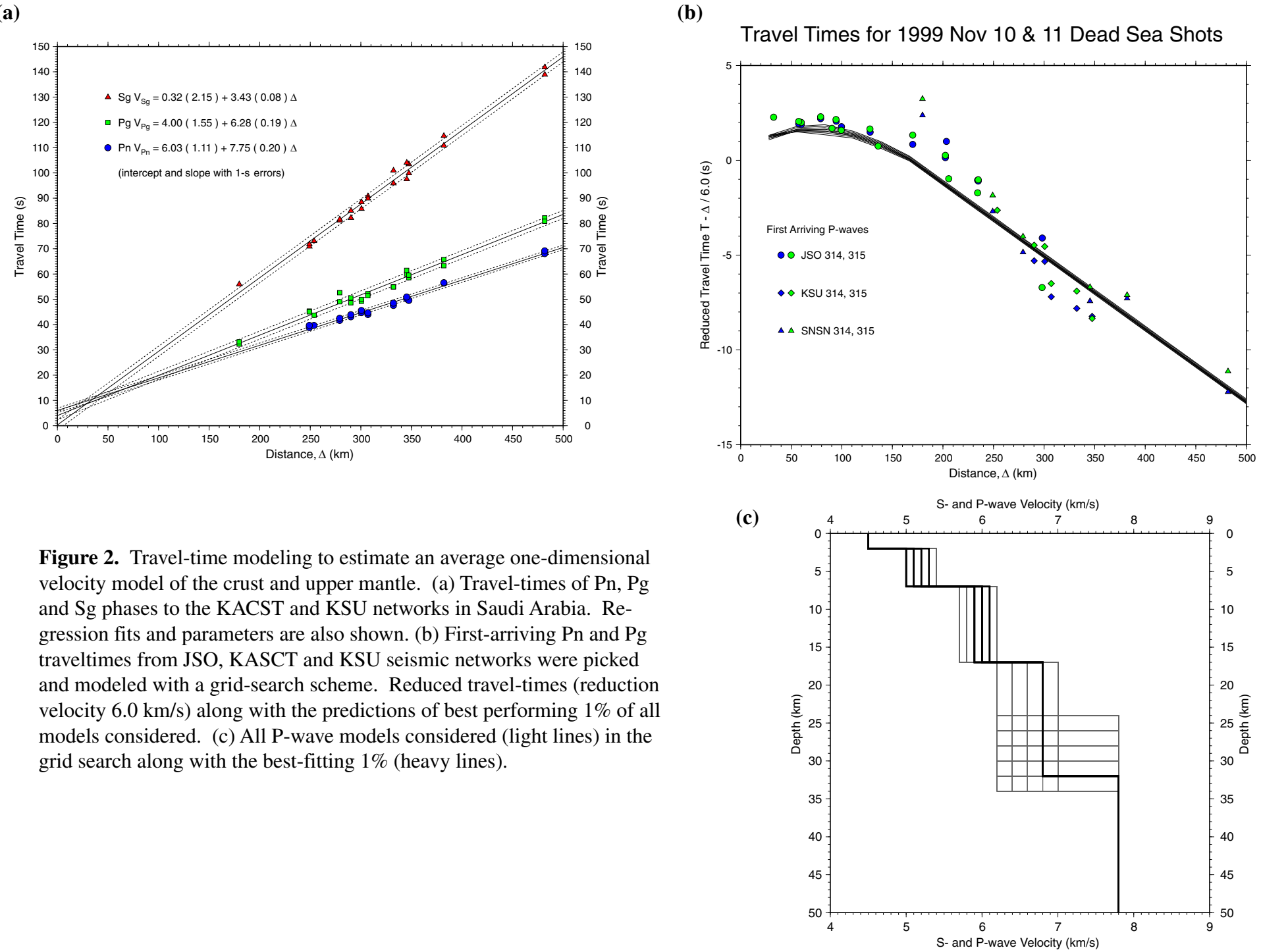

Figure 2. Travel-time modeling to estimate an average one-dimensional velocity model of the crust and upper mantle. (a) Travel-times of Pn, Pg and Sg phases to the KACST and KSU networks in Saudi Arabia. Regression fits and parameters are also shown. (b) First-arriving Pn and Pg traveltimes from JSO, KASCT and KSU seismic networks were picked and modeled with a grid-search scheme. Reduced travel-times (reduction velocity 6.0 km/s) along with the predictions of best performing 1% of all models considered. (c) All P-wave models considered (light lines) in the grid search along with the best-fitting 1% (heavy lines).

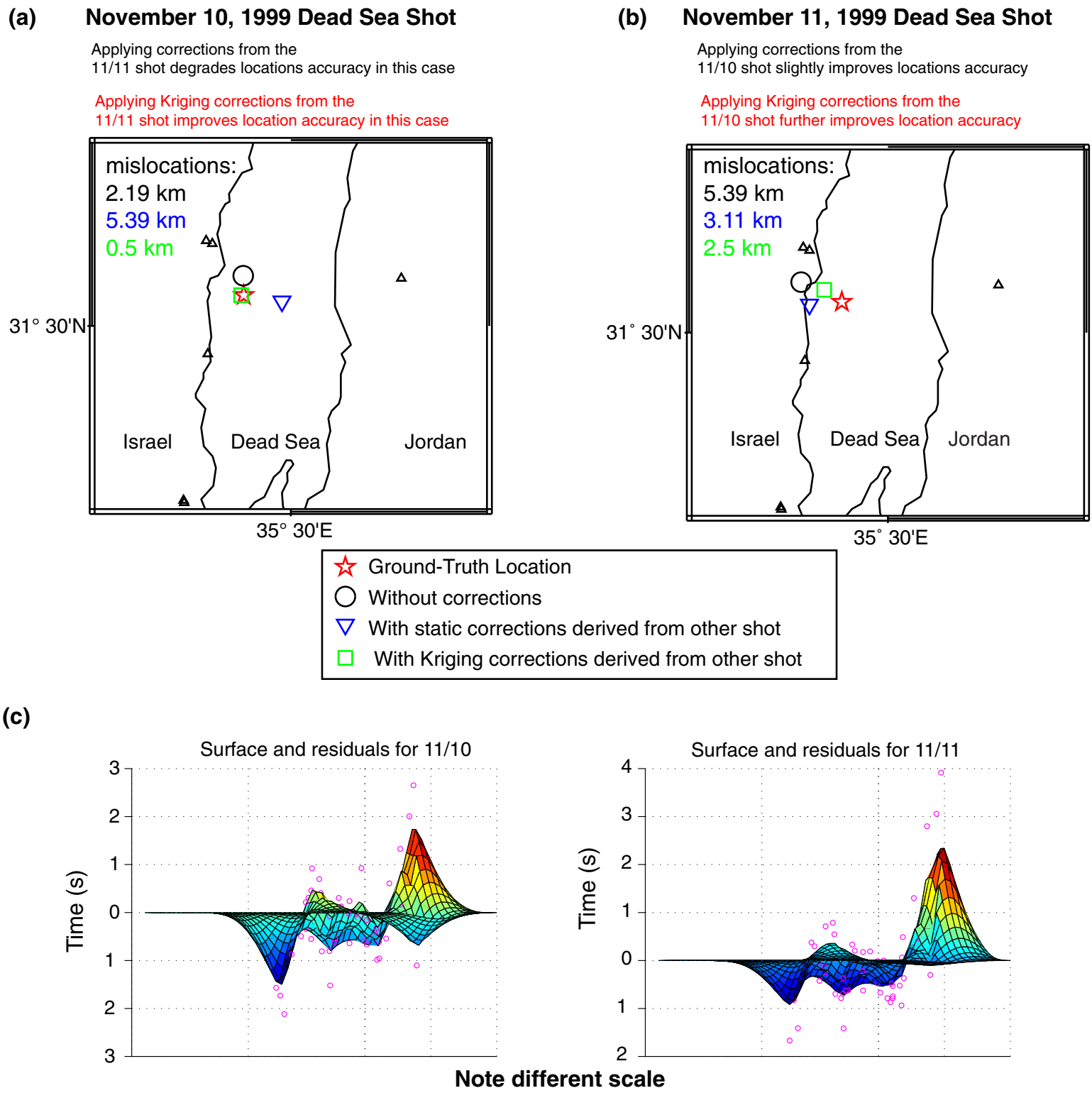

Figure 3. Locations of the (a) November 10, 1999 and (b) November 11, 1999 Dead Sea Shots. Ground truth is shown as the red star. Each shot was located three ways: i) without any path correction (black circle); ii) with static corrections computed as the travel time residual relative to a one-dimensional model (blue triangle); and iii) using travel-time correction computed from the kriging algorithm (green square). The travel-time corrections used to locate each shot were computed from the other shot. (c) Side-view of the travel-time residuals for each shot along with the kriged correction surface. Notice that the patterns of the residuals and the surfaces are very similar, however some residuals at individual stations are not in agreement.

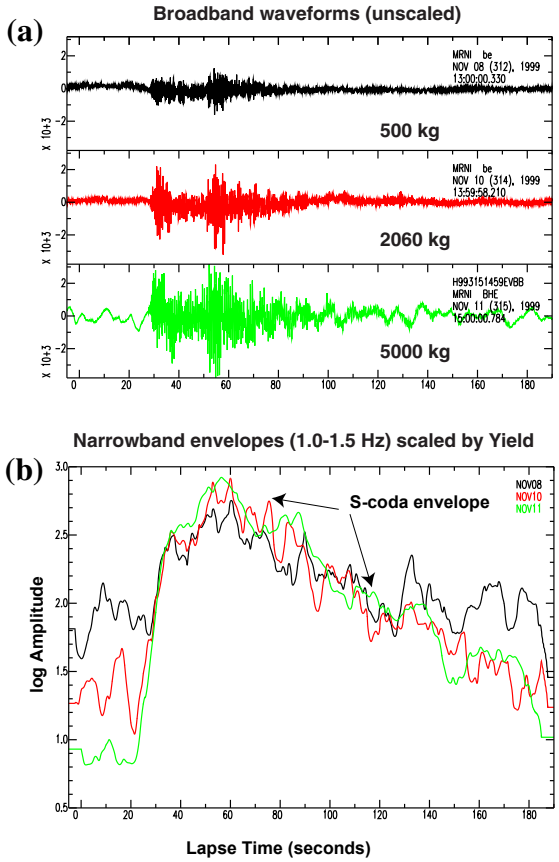

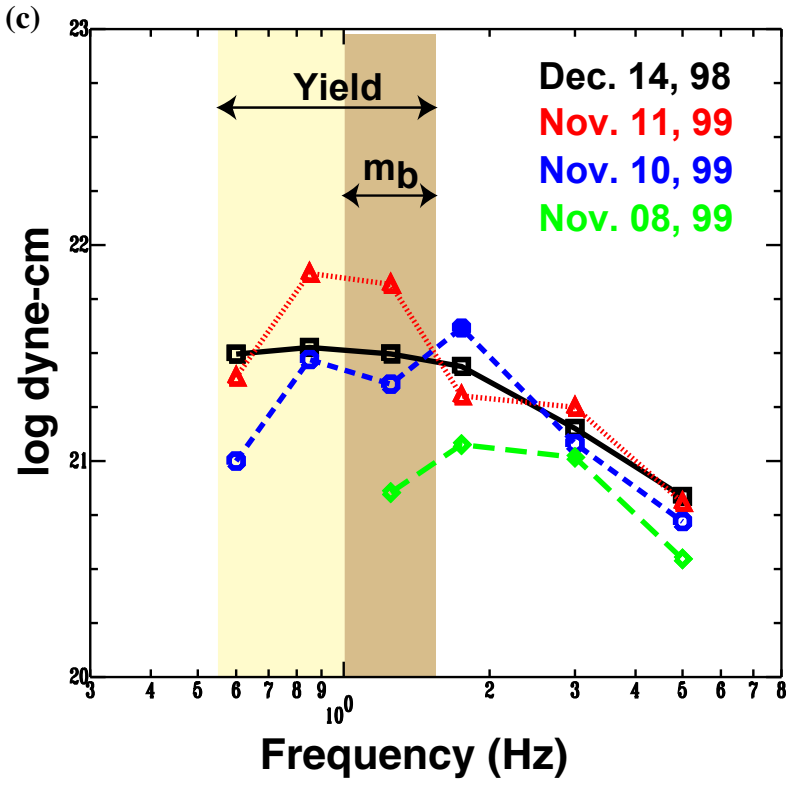

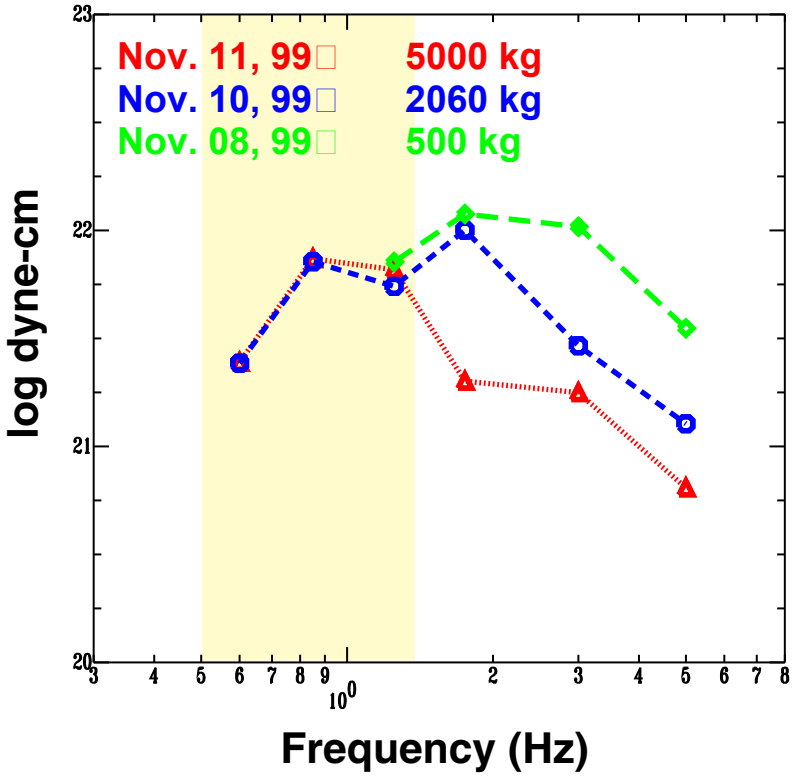

Figure 4. **(a)** Broadband East component waveforms for the three Dead Sea Shots at MRNI (unscaled).

(b) Narrow-band envelopes of the three shots scaled by yield. Notice that the shapes and decay rates of the S-wave coda are quite similar.

(c) Source spectra for the three shots and for an earthquake (M_L 3.6) south of the Dead Sea. Note that the spectrum for each shot is peaked relative to the earthquake spectrum. Spectral peaking arises from interference notches, Rg-to-S scattering and/or near source attenuation effects. Yields of the smaller shots are estimated relative to the 5000 kg shot in the low-frequency band (0.5-1.5 Hz) band to be 2036 kg and 570 kg for the Nov. 10 and Nov. 8 shots. Single-station coda body-wave magnitudes, m_b, are estimated from the 1-2 Hz band: 3.6, 3.45 and 2.95.

(d) Source spectra of the three shots scaled by yield. The spectra are similar for frequencies less than 1.5 Hz, but different for frequencies above 1.5 Hz. This suggests that the corner frequencies of each event are different, possibly due to different effective source diameters.

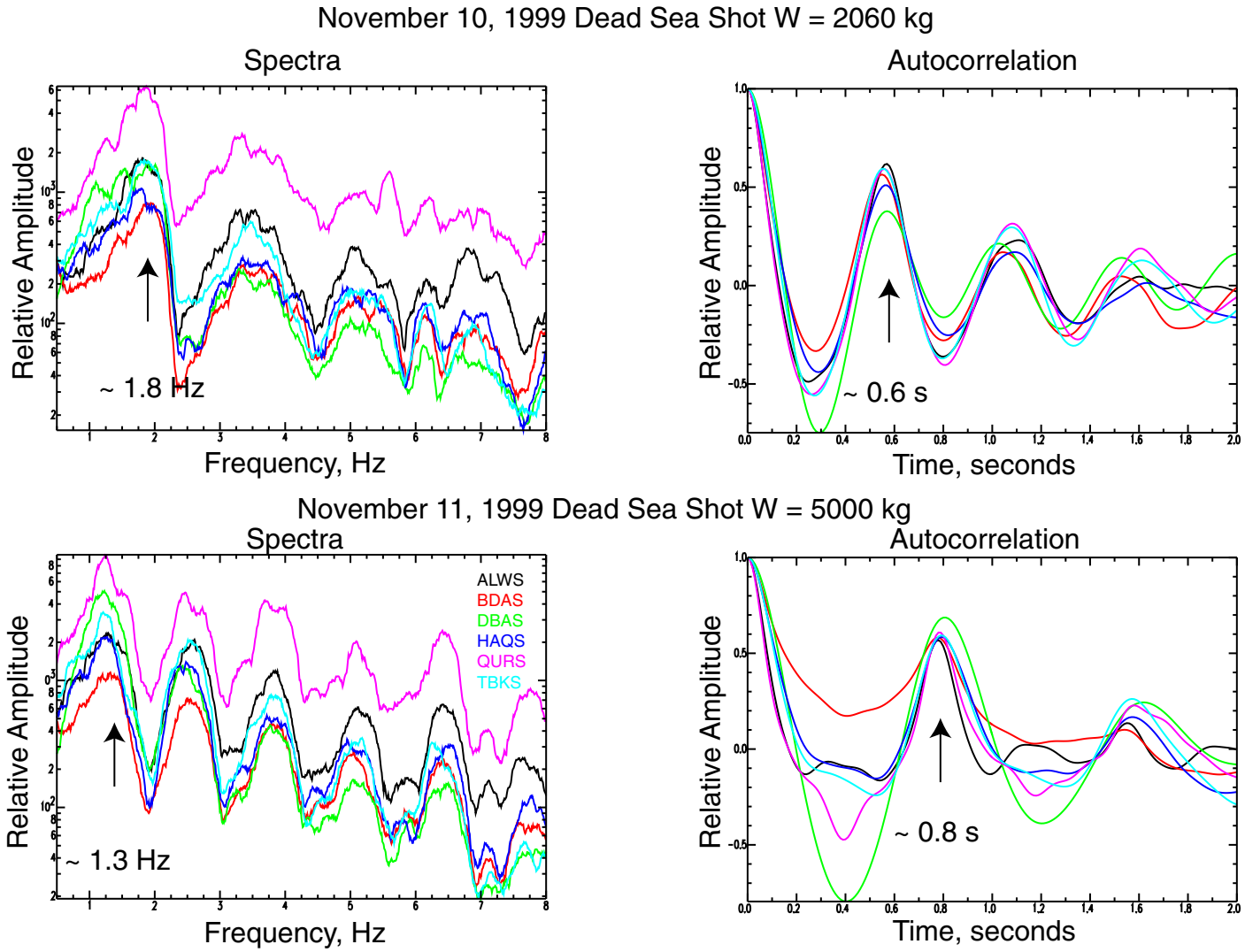

Figure 5. Spectra and auto-correlations of the two largest Dead Sea Shots taken from the vertical component broadband stations of the Saudi National Seismic Network. The scalloping of the spectra (left) is consistent for each shot. Similarly, the auto-correlations (right) of the waveforms are remarkably simlilar. The spectral maxima and peak auto-correlations are consistent with predicted bubble pulse frequencies/periods reported by GII: 1.72 Hz/0.583 s and 1.26 Hz/0.791 s for the November 10 and 11 shots, respectively.